MODIFICATION OF SHAPE MEMORY POLYMERS USING HYDROGENATED METHYLENE DIPHENYL DIISOCYANATE

An Undergraduate Research Scholars Thesis

by

JANE FREDERICK

Submitted to the Undergraduate Research Scholars program
Texas A&M University
in partial fulfillment of the requirements for the designation as an

UNDERGRADUATE RESEARCH SCHOLAR

Approved by
Research Advisor: Dr. Duncan Maitland

May 2016

Major: Biomedical Engineering

TABLE OF CONTENTS

ABSTRACT

Modification of Shape Memory Polymers using Hydrogenated Methylene Diphenyl Diisocyanate

Jane Frederick
Department of Biomedical Engineering
Texas A&M University

Research Advisor: Dr. Duncan Maitland
Department of Biomedical Engineering

A new device based on porous, stimulus-responsive materials is being developed for the treatment of brain aneurysms. Shape memory polymer (SMP) foams can be heated above their transition temperature (T_{trans}) and crimped onto a metal coil to enable delivery through a micro-catheter to the aneurysm. Passive actuation at body temperature allows the foams to expand and occlude the aneurysm to prevent further vessel ballooning. The SMP foams are synthesized by reacting low molecular weight monomers, specifically polyols and polyisocyanates, to generate a highly crosslinked network with shape memory properties. Current material formulations with trimethylhexamethylene diisocyanate (TMHDI) as the primary diisocyanate demonstrate low toughness, which reduces shape recovery after actuation. We hypothesized that modifying the current diisocyanate mixture to contain hydrogenated methylene diphenyl diisocyanate (HMDI) combined with either hexamethylene diisocyanate (HDI) or TMHDI would improve foam strength and toughness. HMDI was successfully used to control mechanical properties while maintaining stable volume recovery. Coupling HMDI with HDI showed the most improvement in toughness and tensile strength while retaining high foam volume recovery.

ACKNOWLEDGEMENTS

I would like to thank Dr. Duncan Maitland for giving me this opportunity and Dr. Sayyeda Hasan for all of her guidance on this project. I would also like to thank Dr. Mary Beth Browning Monroe and Dr. Brandis Keller for their input. Thank you to all of the Biomedical Device Laboratory members for the support I have received throughout the duration of this project.

CHAPTER I

INTRODUCTION

In the United States, one in 50 people suffer from an unruptured cerebral aneurysm, the vast majority of whom experience no symptoms that would lead them to seek medical attention [1, 2]. A cerebral aneurysm occurs when a weak wall on a blood vessel balloons out and fills with blood [3]. Diagnosis of a cerebral aneurysm is often made close to the point of rupture, when immediate medical treatment is required to minimize further vessel ballooning [4]. Approximately 40 % of cases involving ruptured cerebral aneurysms are fatal, and survivors often experience chronic handicap [5, 6]. A device that minimizes the incidence of rupture while promoting stable occlusion is needed, as current treatments are severely limited.

Patients with diagnosed cerebral aneurysms have several treatment options, including surgical clipping, embolization with platinum coils, intracranial stenting, and embolization with a liquid agent [7]. The conventional methods are clipping and endovascular coiling, although both procedures have significant drawbacks. Clipping involves placing a clip across the base of the aneurysm to stop further growth by preventing blood flow into the aneurysm [8]. Surgical clipping is an extremely invasive procedure that involves craniotomy and could cause aneurysm regrowth if slipping of the clip occurs [9, 10]. As an alternative, embolization using bare platinum coils (BPCs) requires occluding the aneurysm using multiple coils until thrombosis is achieved [11]. Improper deployment and coil placement can result in an ischemic stroke if the coils travel down the parent vessel [12-14]. Additionally, the aneurysm could burst after perforation by a coil or recanalize due to coil packing [15-17]. Even though these risks persist,

medical professionals prefer endovascular coiling, as it is minimally invasive and has a higher success rate compared to clipping [18, 19]. Thus, an improvement upon the standard BPC method would provide a better treatment option for aneurysm occlusion while eliminating the need to train physicians on a new device.

The Biomedical Device Laboratory has developed a shape memory polymer (SMP) foam-over-coil device that performs similarly to BPCs. The device can be deployed using a micro-catheter and requires multiple devices to be inserted into the aneurysm [20]. The SMP foam promotes rapid, stable occlusion with a better healing response compared to the BPCs [20, 21]. Additionally, fewer coils are needed to fill the aneurysm, because the porous SMP foam on the device expands to fill more space than a BPC alone, reducing the risk of aneurysm perforation and coil migration [22]. The SMP foam is heated above its transition temperature and crimped onto the coil to ensure a small device geometry [23]. Upon delivery, the foam passively expands due to plasticization and thermal input from the physiological environment [24]. During material processing, the foams may experience micro-tears and loss of tensile strength, causing the device to lose some of its shape recovery properties. Tears in the SMP foams could also occur during device delivery through the micro-catheter, which could result in embolic particles entering the bloodstream. Increasing the foam toughness by changing the diisocyanate composition could increase shape volume recovery as well as reduce the risk of tearing during foam processing. Current device formulations utilize trimethylhexamethylene diisocyanate (TMHDI) to tailor the actuation times to less than 10 minutes and allow adequate time for the physician to implant the device [25]. Changing the foam composition to include hydrogenated methylene diphenyl diisocyanate (HMDI) could potentially increase foam strength and overall shape recovery.

CHAPTER II

METHODS

Synthesis

Foam production began after neat films were synthesized and characterized to test reactivity and thermal properties. Both neat films and foams were fabricated with triethanolamine (TEA) (98%, Sigma Alrich), N,N,N',N'-tetrakis(2-hydroxypropyl)ethylenediamine (HPED) (99%, Sigma-Aldrich), trimethyl-1,6-hexamethylene diisocyanate (TMHDI) (TCI America Inc.), hexamethylene diisocyanate (HDI) (TCI America Inc.), and 4.4'-methylenebis(cyclohexyl isocyanate) (HMDI) (TCI America Inc.). The chemical structures of the monomers used are displayed in Figure 1. For foams, deionized (DI) water, surfactants (DC 198 and DC 5943) (Air Products and Chemicals, Inc.), catalysts (T-131 and BL-22) (Air Products and Chemicals, Inc), and Enovate 245fa Blowing Agent (Honeywell International, Inc) were utilized.

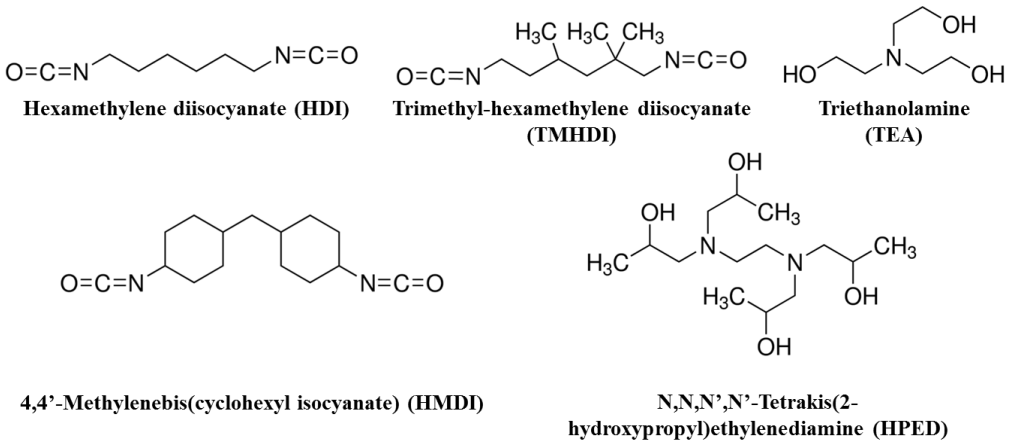

Figure 1. Chemical structures of monomers used in SMP synthesis.

Two series of neat polymer films were fabricated by combining HMDI with either TMHDI or HDI. The polymer solutions were made with predetermined weights of HPED, TEA, HMDI, and TMHDI or HDI, as listed in Table 1 and Table 2. The samples in each series were named 0 HMDI, 10 HMDI, 25 HMDI, and 50 HMDI based on the ratio of HMDI to either HDI or TMHDI. The solutions were then mixed in a speed mixer for 2 minutes and poured into rectangular plastic molds. The molds were placed in a vacuum chamber for 15 minutes to remove air bubbles and were sealed with plastic lids after removal from the chamber. Then, the molds were placed in a pressure chamber under 60 PSI for 24 hours before being placed in an oven to cure at 120 °C for an additional 24 hours. The neat films were taken out of the oven and cooled for testing.

Table 1. Neat polymer film compositions for the HDI series with HMDI.

Sample	**HMDI (wt%)**	**HDI (wt%)**	**HPED (wt%)**	**TEA (wt%)**
0 HMDI	0	56	33	11
10 HMDI	9	49	32	11
25 HMDI	20	39	30	10
50 HMDI	38	24	28	9

Table 2. Neat polymer film compositions for the TMHDI series with HMDI.

Sample	**HMDI (wt%)**	**TMHDI (wt%)**	**HPED (wt%)**	**TEA (wt%)**
0 HMDI	0	62	29	10
10 HMDI	8	55	28	9
25 HMDI	19	45	28	9
50 HMDI	36	29	27	9

Foams were synthesized by first making an isocyanate (NCO) premix with HPED, TEA, HMDI, and TMHDI or HDI. The NCO premix was cured in an oven for 2 days while the temperature

ramped up to 50 °C and then down to room temperature. A hydroxyl (OH) premix was made from the remaining HPED and TEA mixed with DI water and catalysts. The NCO and OH premixes were mixed together with surfactants and the blowing agent in a speedmixer before being poured into a foaming bucket. The bucket was placed into an oven at 90 °C for 20 minutes and then removed and cooled to room temperature. The weights for each component used in foam synthesis are listed in Table 3 and Table 4.

Table 3. Foam compositions for the HDI series with HMDI.

Sample	HMDI (wt%)	HDI (wt%)	HPED (wt%)	TEA (wt%)	Water (wt%)	T-131 (wt%)	BL-22 (wt%)	DC 198 (wt%)	DC 5943 (wt%)	Enovate (pph)
0 HMDI	0	69.85	22.39	7.51	3.07	0.30	0.71	3.73	2.78	6.94
10 HMDI	10.48	60.47	21.60	7.25	3.00	0.34	0.71	3.76	2.83	6.97
25 HMDI	24.83	47.76	20.34	6.85	2.81	0.31	0.71	3.80	2.84	7.03
50 HMDI	45.61	29.23	18.74	6.32	2.56	0.29	0.72	3.79	2.83	7.09

Table 4. Foam compositions for the TMHDI series with HMDI.

Sample	HMDI (wt%)	TMHDI (wt%)	HPED (wt%)	TEA (wt%)	Water (wt%)	T-131 (wt%)	BL-22 (wt%)	DC 198 (wt%)	DC 5943 (wt%)	Enovate (pph)
0 HMDI	0	67.91	17.39	5.96	2.41	0.32	0.66	2.21	3.87	15.07
10 HMDI	8.31	60.03	17.10	5.74	2.40	0.26	0.66	2.16	3.92	15.10
25 HMDI	20.27	48.75	16.35	5.49	2.35	0.26	0.70	2.18	4.22	15.08
50 HMDI	39.12	31.36	15.50	5.21	2.24	0.26	0.66	2.18	3.91	15.19

Cooled foams were cut into smaller blocks and crimped with a Carver Press (Carver, Inc., Wabash, IN) heated to 90 °C. Foams were left in their compressed forms to cool before being cleaned via sonication to remove unreacted monomers, catalysts, and surfactants. Foams were submerged in RO water for a 15 minute sonication cycle and then in isopropyl alcohol (IPA) for two more 15 minute cycles. Finally, the foams were again submerged in RO water for four 15

minute sonication cycles to remove any traces of IPA. The cleaned foams were dried in an oven at 50 °C for 24 hours before characterization.

Characterization

Contact angles

Hydrostatic contact angles were measured for each neat film with a KSV CAM-2008 Contact Angle Analyzer (KSV Instruments Ltd., Helsinki, Finland) by placing a 5 µL drop of reverse osmosis (RO) water on the film (n=3). The drop was analyzed by taking 9 image frames at 15 second intervals and measuring the contact angle for each frame with the Attension Theta software package (Biolin Scientific, Stockholm, Sweden). The average contact angle was found from the frames. The RO water contact angle for each neat film was found from the average of the three measured contact angles.

Density and pore characteristics

The density of each foam was found by cutting cubes out of the top, middle, and bottom of the foams with a wire cutter. The mass, length, width, and height of each cube was found, and the density was calculated in g/cm^3. Thin square sections were cut in the axial and transverse directions of the foams and sputter coated with gold particles for 60 seconds with a Cressington Sputter Coater (Ted Pella, Inc., Redding, CA) at 20 mA. Images of each foam section were taken at 11x magnification under vacuum with a Joel NeoScope JCM-5000 scanning electron microscope (SEM) (Nikon Instruments, Inc., Melville, NY). The images were analyzed with ImageJ software (NIH, Bethesda, MD) to calculate average pore size and isotropicity.

Fourier transform infrared (FTIR) spectroscopy

FTIR spectra of each sample was obtained by cutting thin rectangular sections from the foam and analyzing them with a Bruker ALPHA Infrared Spectrometer (Bruker, Billerica, MA). The FTIR spectra were collected by taking 32 background scans and 64 sample scans at a 4 cm^{-1} resolution in absorption mode. The collected spectra were corrected using OPUS software (Bruker, Billerica, MA) to remove the background scans and to perform a baseline correction and an atmospheric compensation.

Differential scanning calorimetry (DSC)

Five foam pieces (4-6 mg) were cut and placed in an aluminum tin to find the dry glass transition temperature (T_g). The aluminum tins with the foam samples were placed in a Q-200 DSC (TA Instruments, Inc., New Castle, DE) to find the thermogram for each composition. The DSC procedure involved an initial cycle wherein temperature was decreased down to -40 °C at 10 °C per minute and held for 2 minutes. Then, the temperature was increased at a rate of 10 °C per minute up to 150 °C where it was again held constant for 2 minutes. The next cycle decreased the temperature at 10 °C per minute to -40 °C, where the temperature was held constant for 2 minutes, before increasing it back to 150 °C at a rate of 10 °C per minute. The second cycle was used to find dry T_g from the inflection point on the thermal transition curve for each of the five samples with TA instruments software (TA Instruments, Inc., New Castle, DE). Three samples (4-6 mg) were cut and placed in RO water to find wet T_g. The lower HMDI concentration foam samples were submerged in 50 °C RO water for 10 minutes, while the higher concentrations were placed in 100 °C RO water for 10 minutes to ensure plasticization of the foams. The samples were then placed on a Kim Wipe (Kimberly-Clark Professionals, Roswell, GA) and

pressed with the Carver Press to remove excess moisture. An aluminum tin with a vented lid was then filled with the dried foam and placed in a Q-200 DSC. The samples were cooled to -40 °C, held at this temperature for 2 minutes, and heated to 120 °C at a rate of 10 °C per minute. The inflection point of the thermogram was found using TA instruments software to find the wet T_g of the samples.

Thermal gravimetric analysis (TGA)

Small foam samples were cut and placed in a ceramic pan to measure thermal stability. The ceramic pan was placed on an aluminum pan and run through a cycle in a Q-50 TGA (TA Instruments, New Castle, DE) to find mass loss. The procedure used for the TGA involved ramping the oven to 800 °C at a rate of 10 °C per minute with a gas switch from air to nitrogen at 600 °C. The mass loss curves were obtained three times for each composition.

Mechanical testing

Mechanical properties of the foams were found by cutting dog bone-shaped samples with a width of 3 mm and attaching them to wooden stubs. The foam thickness was measured at three points before attaching the stubs to two metal clamps for uniaxial tensile loading tests. The Insight 30 Material Tester (MTS) (MTS Systems Corporation, Eden Prairie, MN) strained the foam until failure at a constant strain rate of 5 $mm \cdot min^{-1}$ and the tensile strength and toughness were found from the stress-strain curve for each composition.

Foam expansion and volume recovery

Foam blocks (10 mm in length) were used to cut cylindrical foam samples (3 per composition) with a 4 mm biopsy punch. Samples were threaded onto a 203.20 µm nitinol wire (NDC, Fremont, CA). The foams were then placed in a ST 150-42 stent crimper (Machine Solutions, Flagstaff, AZ) to radially crimp the foams to a small diameter by heating the foams to 100 °C, holding the temperature for 15 minutes, and cooling them back down to room temperature. An image was taken of the initial foam diameter before placing the foams in a 40 °C water bath for 10 minutes, with images taken every minute. Foams were then submerged in a 70 °C water bath before being moved into a 100 °C, each for 10 minutes with images taken every minute. The images were then analyzed with ImageJ software to find the initial and final diameters to determine foam volume recovery from Equation 1 and expansion from Equation 2.

$$Volume\ recovery = \left(\frac{Recovered\ diameter}{Original\ diameter}\right)^2 \times 100\% \qquad \text{Equation 1}$$

$$Volume\ expansion = \left(\frac{Recovered\ diameter}{Compressed\ diameter}\right)^2 \qquad \text{Equation 2}$$

CHAPTER III

RESULTS

Characterization

Contact angles

Hydrostatic contact angles from the neat films of the HDI and TMHDI series are shown in Tables 5 and Table 6, respectively. While the HDI series showed a slight increase in contact angles with increasing HMDI, the TMHDI had no change in hydrophobicity. The addition of HMDI had a slight effect on the hydrophobicity of the HDI neat polymer film due to the addition of two hydrophobic cyclohexyl rings. The lack of effect on TMHDI films can be explained by the nonpolar methyl groups, which have similar hydrophobicity to that of HMDI.

Table 5. Density and contact angles for the HDI series with varied HMDI content.

Sample	**Density ($g \cdot cm^{-3}$)**	**Contact Angle (°)**
0 HMDI	0.0164 ± 0.0007	60 ± 7
10 HMDI	0.0176 ± 0.0003	59 ± 8
25 HMDI	0.0220 ± 0.0002	74 ± 0.1
50 HMDI	0.0496 ± 0.0020	66 ± 5

Table 6. Density and contact angles for the TMHDI series with varied HMDI content.

Sample	Density ($g \cdot cm^{-3}$)	Contact Angle (°)
0 HMDI	0.0129 ± 0.0004	80 ± 5
10 HMDI	0.0132 ± 0.0010	87 ± 10
25 HMDI	0.0184 ± 0.0024	78 ± 1
50 HMDI	0.0201 ± 0.0010	79 ± 8

Density and pore characteristics

Introduction of HMDI into the foams increased foam density from 16.4 mg cm^{-3} to 49.6 mg cm^{-3} in the HDI series and from 12.9 mg cm^{-3} to 22.5 mg cm^{-3} in the TMHDI series (Tables 5 and 6, respectively). The increase in density can be correlated with the decreased pore sizes shown in Tables 7 and 8. Increased quantities of HMDI increased pore isotropicity in the HDI series and had no effect on isotropicity in the TMHDI series (Tables 7 and 8, respectively).

Table 7. Pore sizes for the HDI series with varied HMDI content.

Sample	Axial Pore Size (μm)	Transverse Pore Size (μm)	Isotropicity (%)
0 HMDI	2630 ± 390	1670 ± 210	63
10 HMDI	1840 ± 150	820 ± 90	45
25 HMDI	1910 ± 190	890 ± 100	46
50 HMDI	360 ± 60	300 ± 50	83

Table 8. Pore sizes for the TMHDI series with varied HMDI content.

Sample	Axial Pore Size (μm)	Transverse Pore Size (μm)	Isotropicity (%)
0 HMDI	1670 ± 230	950 ± 120	57
10 HMDI	1920 ± 320	950 ± 130	49
25 HMDI	1410 ± 160	1540 ± 160	91
50 HMDI	1510 ± 260	800 ± 90	53

Figure 2 shows a comparison between axial and transverse pore sizes in both the HDI and TMHDI series. Shrinking of pores occurred as a result of the stiff structure of HMDI, which stacks close together to form smaller struts and cells, thereby increasing the density within a unit area. The flexibility of HDI allows it to bend to create larger pores, while TMHDI has limited pliability due to the methyl side groups that restrict the strut length. As a result, the addition of HMDI had a larger effect on the cell structure of HDI compared to that of TMHDI.

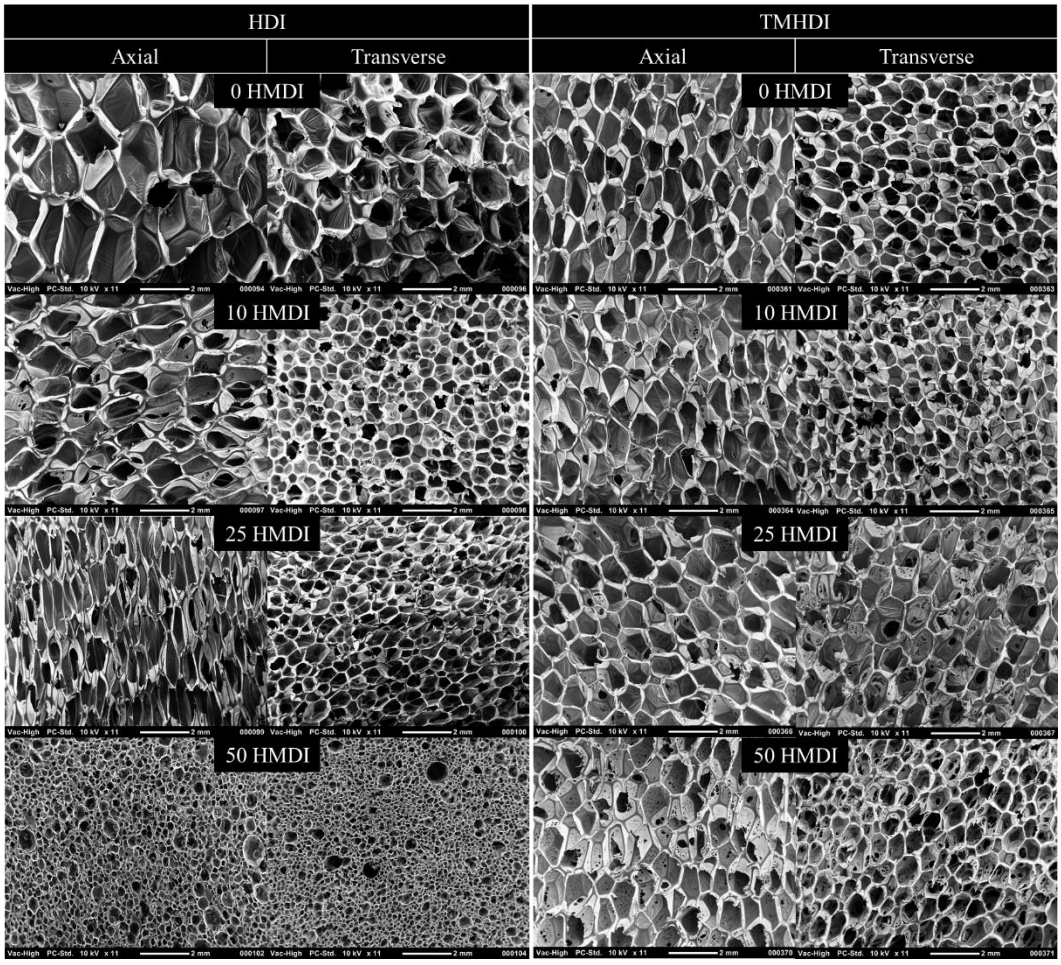

Figure 2. SEM images of foam pores at 11x magnification and 10 kV under vacuum.

Fourier transform infrared (FTIR) spectroscopy

Inspection of the FTIR spectra collected from both the HDI and TMHDI series showed the characteristic C=O stretch peak at 1698 cm^{-1} of a polyurethane (Figures 2 and 3). The C=O stretch shoulder at 1647 cm^{-1} identifies the urea links formed by isocyanates reacting with water during foaming. Addition of HMDI decreased the strength of the C-H bend peak at 1465 cm^{-1} in TMHDI, which occurs as a result of methyl groups. In HDI, the C-H bend peak remained relatively unchanged due to the lack of methyl groups in both HDI and HMDI. At 1307 cm^{-1}, the C-N stretch peak increased in relation to the concentration of HMDI in both HDI and TMHDI

due to better incorporation of HMDI into the matrix. Due to the C-C stretch of the carbon backbone at 1252 cm^{-1}, the C-N stretch of each composition requires more energy to excite the bond, causing a shift from the original position of the peak between 1020 cm^{-1} to 1250 cm^{-1}. The N-H stretch of an amine located at 3330 cm^{-1} demonstrates both secondary and tertiary amines in the polymer structure. Finally, the C-H stretch at 3000 cm^{-1} that is characteristic of cyclic groups becomes more defined upon addition of HMDI in both HDI and TMHDI, demonstrating successful incorporation of HMDI.

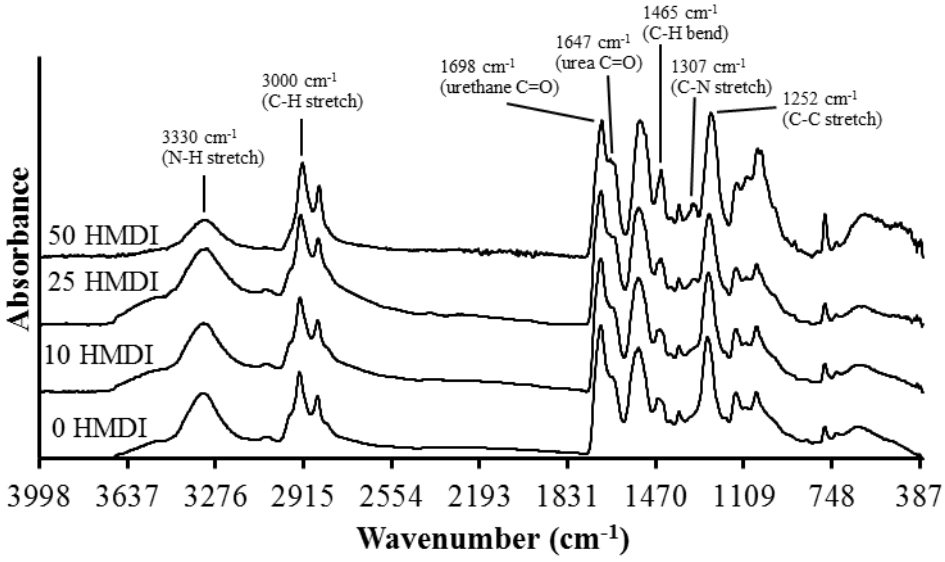

Figure 3. Comparison of FTIR spectra of the foams in the HDI series.

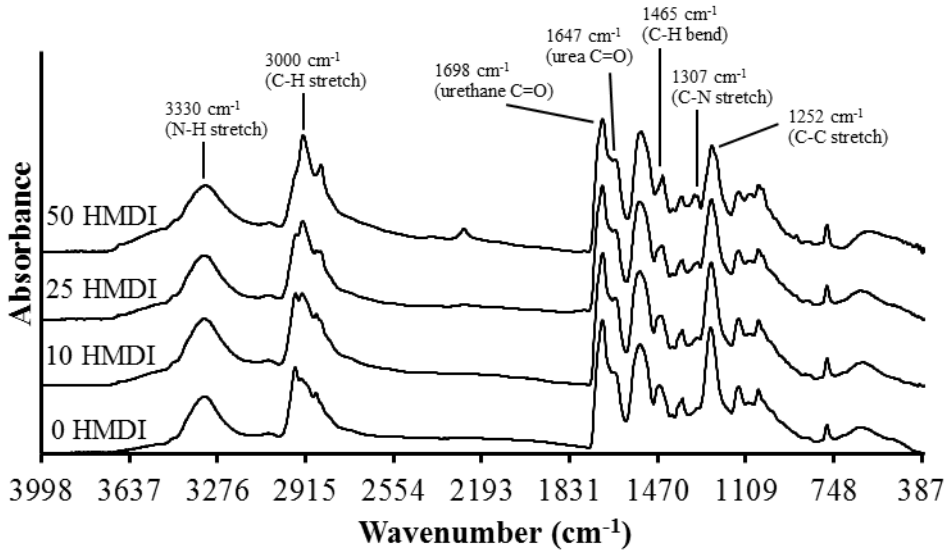

Figure 4. Comparison of FTIR spectra from the foams in the TMHDI series.

Differential scanning calorimetry (DSC)

Changes in thermal transition properties with increasing HMDI concentration found from thermogram analysis are listed in Tables 9 and 10. Incorporation of HMDI increased the dry T_g from 51 °C to 107 °C for HDI foams and 68 °C to 113 °C for HDI foams. The drastic increases in T_g result from the stiffness of HMDI, which can only rotate freely around the central carbon. Thus, HMDI packs closely together due to the lack of flexibility to create a more crystalline material, increasing the relative T_g of the foams. In contrast, HDI has a free carbon backbone with no side groups, which allows it to rotate around each of the carbons with little steric hindrance. TMHDI contains the same carbon backbone of HDI, with the addition of three methyl side groups which increase steric hindrance and the rotational ability of the compound. As a result, the high flexibility of HDI results in a low T_g, while increased steric hindrance from side groups give a higher T_g in TMHDI. The addition of the stiff HMDI group effectively increases crystallinity in both foam series, causing large increases in T_g. Correspondingly, the wet T_g of

HDI foams increased from 24 °C to 47 °C, while the wet T_g of TMHDI increased from 44 °C to 47 °C with the addition of HMDI. The relatively small change in wet T_g can be attributed to the similarity in flexibility of polymer chains after plasticization with water. HDI alone had a low T_g due to the original flexibility of the carbon backbone and low steric hindrance. The wet T_g of TMHDI showed only a slight increase with the incorporation of HMDI, suggesting that polymer chains made of a mix of TMHDI and HMDI are similarly flexible as chains made of TMHDI alone after plasticization.

Table 9. Dry and wet T_g for the HDI series with varied HMDI content.

Sample	**Dry T_g (°C)**	**Wet T_g (°C)**
0 HMDI	51 ± 10	24 ± 2
10 HMDI	58 ± 4	45 ± 1
25 HMDI	76 ± 10	47 ± 3
50 HMDI	107 ± 6	47 ± 2

Table 10. Dry and wet T_g for the TMHDI series with varied HMDI content.

Sample	**Dry T_g (°C)**	**Wet T_g (°C)**
0 HMDI	68 ± 2	44 ± 1
10 HMDI	76 ± 3	52 ± 1
25 HMDI	86 ± 6	43 ± 1
50 HMDI	113 ± 5	47 ± 3

Thermal gravimetric analysis (TGA)

Thermal degradation curves for both the HDI series and the TMHDI series showed minimal change with increasing concentrations of HMDI (Figures 5 and 6, respectively). All foams experienced thermal decomposition at 350 °C, due to the presence of urethane and urea bonds in each composition. The chemical structure of HMDI had no effect on foam thermal stability, as HMDI forms the same types of bonds and crosslinks as TMHDI and HDI.

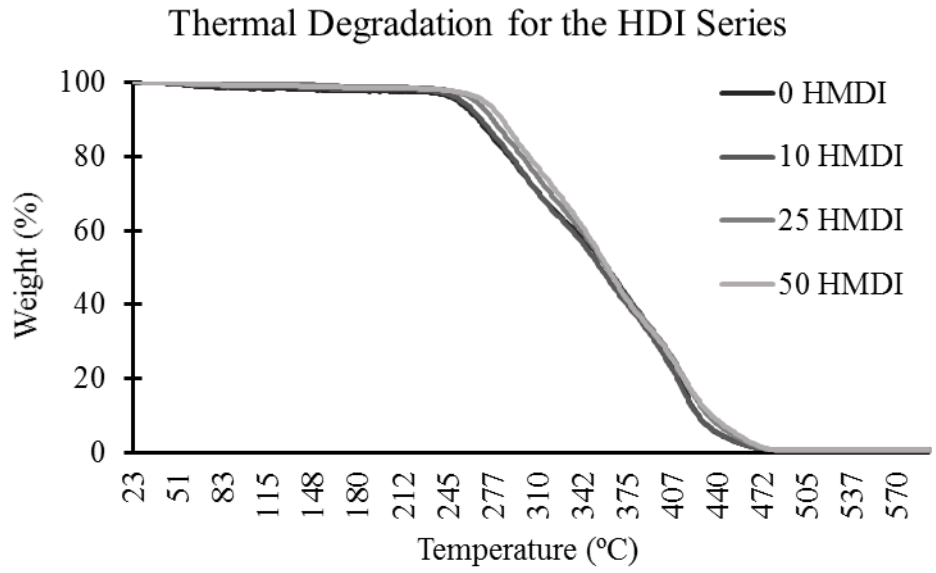

Figure 5. Comparison of thermal stability for the HDI series with varied HMDI content.

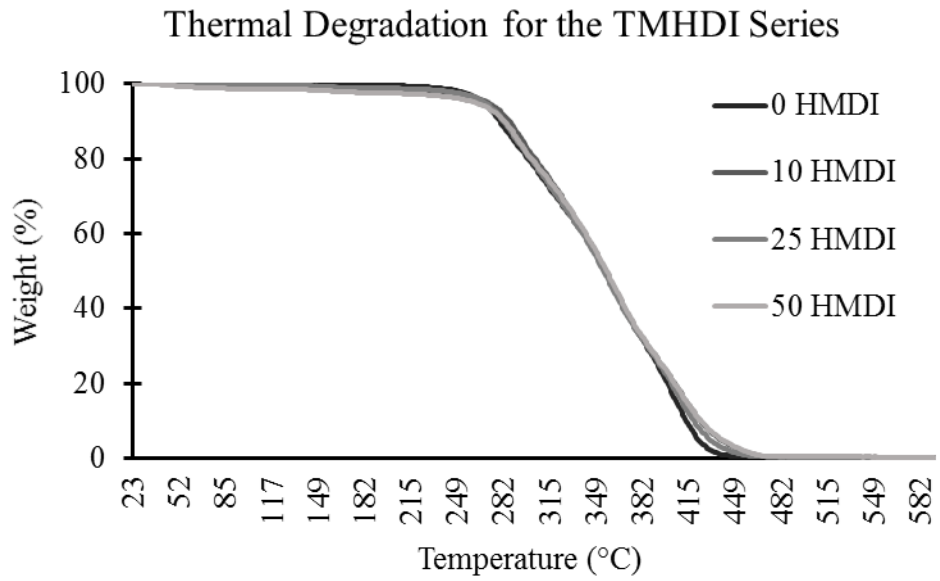

Figure 6. Comparison of thermal stability for the TMHDI series with varied HMDI content.

Mechanical testing

With increased HMDI concentration, opposing trends occur in the mechanical properties of the HDI series and TMHDI series (Tables 11 and 12, respectively). Incorporation of HMDI into HDI-based compositions increased foam toughness from 18 $J \cdot m^{-3}$ to 52 $J \cdot m^{-3}$ and ultimate tensile strength from 51 kPa to 219 kPa. In comparison, TMHDI-based foam toughness decreased from 69 $J \cdot m^{-3}$ to 32 $J \cdot m^{-3}$ and tensile strength decreased from 161 kPa to 122 kPa with HMDI incorporation. Strain at break decreased with HMDI incorporation for both foam series, with the exception of a few outliers. With HMDI incorporation, HDI foam strain at break decreased from 41% to 27%, while TMHDI foam strain at break decreased from 53% to 21%.

Table 11. Summary of key mechanical properties for the HDI series with varied HMDI content.

Sample	Toughness ($J \cdot m^{-3}$)	Ultimate Tensile Strength (kPa)	Strain at Break (%)
0 HMDI	18 ± 6	51 ± 14	41 ± 11
10 HMDI	22 ± 4	66 ± 5	55 ± 11
25 HMDI	34 ± 12	114 ± 32	35 ± 11
50 HMDI	52 ± 10	219 ± 64	27 ± 7

Table 12. Summary of key mechanical properties for the TMHDI series with varied HMDI content.

Sample	Toughness ($J \cdot m^{-3}$)	Ultimate Tensile Strength (kPa)	Strain at Break (%)
0 HMDI	68.85 ± 11.71	161.27 ± 41.37	53 ± 14
10 HMDI	44.05 ± 15.70	139.23 ± 34.22	36 ± 6
25 HMDI	40.57 ± 10.28	129.10 ± 34.85	38 ± 6
50 HMDI	32.40 ± 6.53	122.27 ± 36.60	21 ± 4

The increase in toughness and tensile strength in the HDI series is due to the relative flexibility of the HDI and HMDI chemical structures. HDI has no side groups or bulky groups that restrict movement, allowing it to rotate freely and form a ductile polymer. Addition of the inflexible HMDI cyclohexyl rings forms a stiff polymer that resists deformation, making the polymer tougher and stronger while maintaining ductility from the HDI. In contrast, the methyl side groups of TMHDI render it relatively inflexible. Addition of stiff HMDI to TMHDI creates a stiffer, more brittle structure that breaks before increased deformation occurs, reducing the

toughness, tensile strength, and strain at break. Figures 7, 8, and 9 display the comparison of trends in the mechanical properties for both the HDI and TMHDI series.

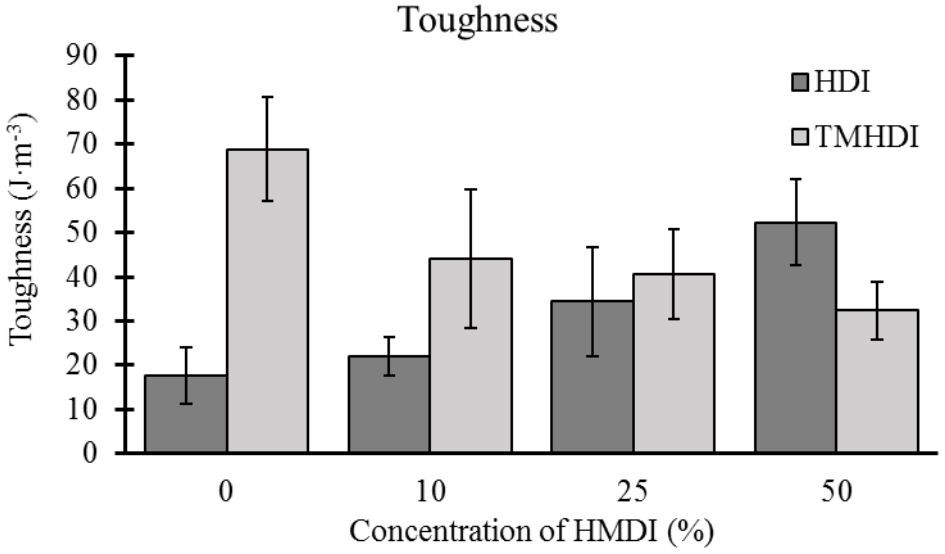

Figure 7. Comparison of toughness for both HDI and TMHDI series with varied HMDI content.

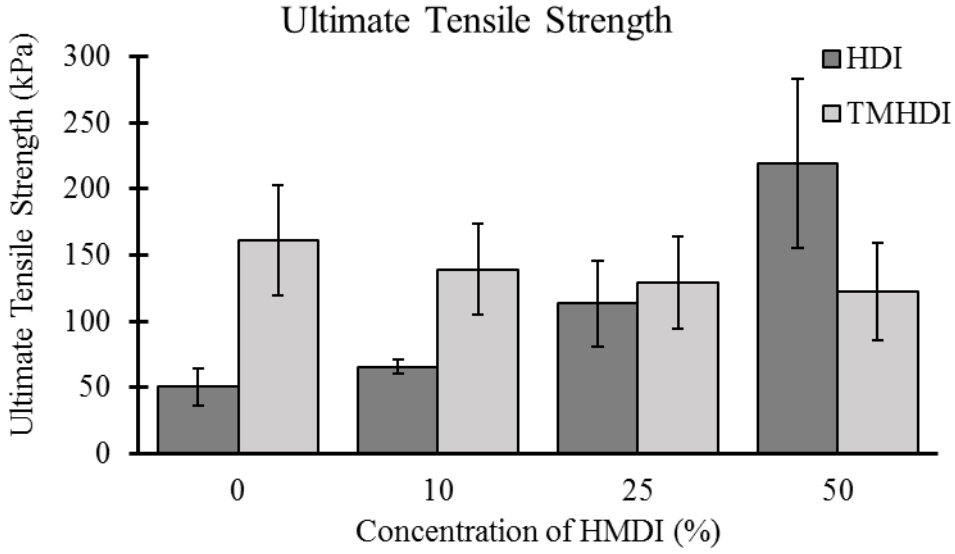

Figure 8. Comparison of ultimate tensile strength for both HDI and TMHDI series with varied HMDI content.

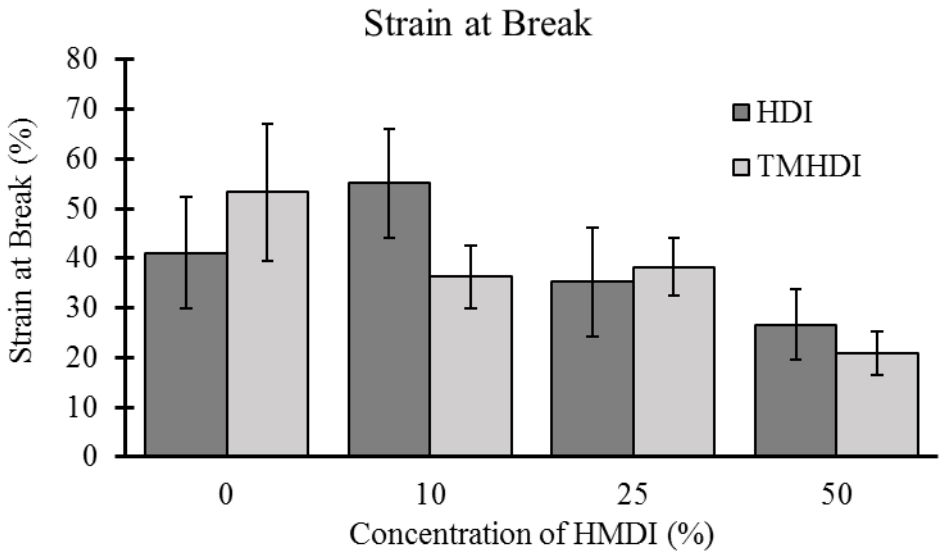

Figure 9. Comparison of percent strain at break for both HDI and TMHDI series with varied HMDI content.

Foam expansion and volume recovery

Volume expansion and recovery after foam actuation in RO water decreased while the temperature at which actuation occurred increased (Tables 13 and 14). The pure HDI foams showed 23-fold expansion compared to 16-fold for the foam with the highest HMDI concentration. The percent volume recovery for the HDI series shows a steady decreasing trend from 92% to below 77% with increasing HMDI concentration; however the highest HMDI concentration foam acts an outlier due to difficulty with heating above its dry T_g to properly crimp the foam. Volume expansion in TMHDI decreased from 23-fold to 8-fold, and volume recovery decreased from 71% to 35% with the addition of HMDI. In total, all foams expanded between 8-fold to 23-fold after placement in warm RO water and maintained greater than 35% shape volume recovery.

Table 13. Summary of key shape recovery properties after actuation in 100 °C RO water for the HDI series with varied HMDI content.

Sample	Volume Expansion (x)	Volume Recovery (%)
0 HMDI	23 ± 5	92 ± 19
10 HMDI	22 ± 4	82 ± 15
25 HMDI	17 ± 5	77 ± 15
50 HMDI	16 ± 3	91 ± 8

Table 14. Summary of key shape recovery properties after actuation in 100 °C RO water for the TMHDI series with varied HMDI content.

Sample	Volume Expansion (x)	Volume Recovery (%)
0 HMDI	23 ± 6	71 ± 20
10 HMDI	23 ± 8	66 ± 17
25 HMDI	17 ± 5	49 ± 8
50 HMDI	8 ± 2	35 ± 6

Actuation profiles of the foams in 40 °C, 70 °C, and 100 °C water for both the HDI and TMHDI series are displayed in Figure 10 and Figure 11. The HDI foam without HMDI actuated at 40 °C, while the foam with the highest HMDI concentration actuated at 100 °C. In the TMHDI series, lower HMDI concentration foams actuated at 70 °C and higher concentration foams only began expanding at 100 °C, leading to the low volume recovery indicated in Table 14.

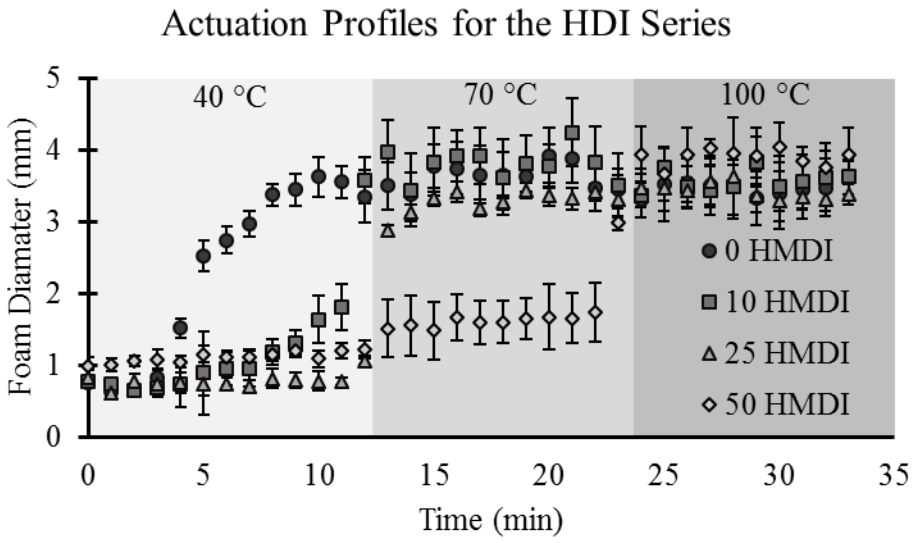

Figure 10. Comparison of actuation profiles for the HDI series with varied HMDI content.

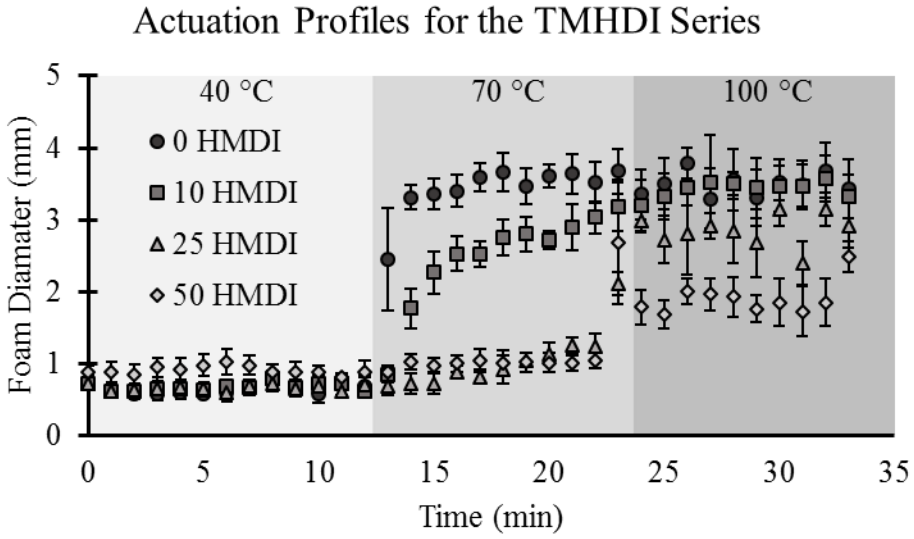

Figure 11. Comparison of actuation profiles for the TMHDI series with varied HMDI content.

CHAPTER IV

CONCLUSION

SMP foams and neat polymer films with a mixture of HMDI and HDI or TMHDI were successfully synthesized. Inspection of the neat polymer film contact angles demonstrated no change in hydrophobicity as a result of change in HMDI concentration. Densities of SMP foams synthesized with HMDI were larger than the original HDI or TMHDI foams, while still in the ultralow range required for a porous, lightweight foam. HDI foam pores became increasingly smaller and more isotropic upon consequent increases in HMDI concentration, while TMHDI pores remained relatively similar in size and isotropicity. Analysis of FTIR spectra clearly demonstrated increased incorporation of HMDI into the HDI and TMHDI matrices. Increasing concentrations of HMDI drastically increased the T_g to above 100 °C in both series due to reduced bond flexibility of the isocyanate monomers. Thermal stability curves found from TGA demonstrated similar thermal degradation for all compositions.

Addition of HMDI to the isocyanate composition of the SMP foams can be successfully be used to modify foam mechanical properties. HDI and HMDI compositions specifically showed improvement in both toughness and ultimate tensile strength compared to TMHDI and HMDI compositions while retaining volume recovery above 77%. Thus, HMDI can be used to generate a more robust foam that resists micro-tearing during delivery of the SMP foam-over-coil device to the aneurysm site. The resulting device will benefit from stronger, more fracture resistant foams which actuate readily inside the body to reduce the amount of coils delivered to pack the

aneurysm. Tough SMP foams made with HMDI will increase the efficiency of the foam-over-coil device while making the device safer for patients.

REFERENCES

1. Thompson, B.G., et al., *Guidelines for the Management of Patients With Unruptured Intracranial Aneurysms: A Guideline for Healthcare Professionals From the American Heart Association/American Stroke Association.* Stroke, 2015.

2. Toshio Nakagawa and Kazuo Hashi, *The incidence and treatment of asymptomatic, unruptured cerebral aneurysms.* Journal of Neurosurgery, 1994. **80**(2): p. 217-223.

3. *What You Should Know About Cerebral Aneurysms*. 2012 October 23, 2012; Available from: www.strokeassociation.org.

4. Juvela, S., K. Poussa, and M. Porras, *Factors Affecting Formation and Growth of Intracranial Aneurysms: A Long-Term Follow-Up Study.* Stroke, 2001. **32**(2): p. 485-491.

5. *Understanding: Brain Aneurysm Statistics and Facts*. 2015 3 September 2015; Available from: www.bafound.org.

6. Winn, H.R., et al., *The long-term prognosis in untreated cerebral aneurysms: II. Late morbidity and mortality.* Annals of Neurology, 1978. **4**(5): p. 418-426.

7. Soni, D. *Treatment Options for Cerebral Aneurysms*. 2003 August, 2009; Available from: www.aans.org.

8. Mckissok, W.R., Alan; Walsh, Lawrence, *Middle Cerebral Aneurysms Further Results in the Controlled Trial of Conservative and Surgical Treatment of Ruptured Intracranial Aneurysms.* The Lancet, 1962. **280**(7253): p. 417-421.

9. Teresa Lin, Allan J. Fox, and Charles G. Drake, *Regrowth of aneurysm sacs from residual neck following aneurysm clipping.* Journal of Neurosurgery, 1989. **70**(4): p. 556-560.

10. Carlos A. David, et al., *Late angiographic follow-up review of surgically treated aneurysms.* Journal of Neurosurgery, 1999. **91**(3): p. 396-401.

11. Fernando Viñuela, Gary Duckwiler, and Michel Mawad, *Guglielmi detachable coil embolization of acute intracranial aneurysm: perioperative anatomical and clinical outcome in 403 patients.* Journal of Neurosurgery, 1997. **86**(3): p. 475-482.

12. Pelz, D.M., S.P. Lownie, and A.J. Fox, *Thromboembolic events associated with the treatment of cerebral aneurysms with Guglielmi detachable coils.* American Journal of Neuroradiology, 1998. **19**(8): p. 1541-7.

13. Colin P. Derdeyn, et al., *Postprocedure ischemic events after treatment of intracranial aneurysms with Guglielmi detachable coils.* Journal of Neurosurgery, 2002. **96**(5): p. 837-843.

14. Rordorf, G., et al., *Silent Thromboembolic Events Associated with the Treatment of Unruptured Cerebral Aneurysms by Use of Guglielmi Detachable Coils: Prospective Study Applying Diffusion-weighted Imaging.* American Journal of Neuroradiology, 2001. **22**(1): p. 5-10.

15. Menno Sluzewski, et al., *Rupture of intracranial aneurysms during treatment with Guglielmi detachable coils: incidence, outcome, and risk factors.* Journal of Neurosurgery, 2001. **94**(2): p. 238-240.

16. Motoharu Hayakawa, et al., *Natural history of the neck remnant of a cerebral aneurysm treated with the Guglielmi detachable coil system.* Journal of Neurosurgery, 2000. **93**(4): p. 561-568.

17. Yuichi Murayama, et al., *Guglielmi Detachable Coil embolization of cerebral aneurysms: 11 years' experience.* Journal of Neurosurgery, 2003. **98**(5): p. 959-966.

18. Molyneux, A., *International Subarachnoid Aneurysm Trial (ISAT) of neurological clipping versys endovascular coiling in 2143 patients with ruptured intracranial aneurysms: a randomised trial.* The Lancet, 2002. **360**(9342): p. 1267-1274.

19. Claiborne Johnston, S., et al., *Endovascular and surgical treatment of unruptured cerebral aneurysms: Comparison of risks.* Annals of Neurology, 2000. **48**(1): p. 11-19.

20. Boyle, A.J., et al., *In vitro and in vivo evaluation of a shape memory polymer foam-over-wire embolization device delivered in saccular aneurysm models.* Journal of Biomedical Materials Research Part B: Applied Biomaterials, 2015: p. n/a-n/a.

21. Rodriguez, J.N., et al., *In vivo response to an implanted shape memory polyurethane foam in a porcine aneurysm model.* Journal of Biomedical Materials Research Part A, 2014. **102**(5): p. 1231-1242.

22. Rodriguez, J.N., et al., *Design and biocompatibility of endovascular aneurysm filling devices.* Journal of Biomedical Materials Research Part A, 2015. **103**(4): p. 1577-1594.

23. Rodriguez, J.N., et al., *Opacification of Shape Memory Polymer Foam Designed for Treatment of Intracranial Aneurysms.* Annals of Biomedical Engineering, 2011. **40**(4): p. 883-897.

24. Nash, L.D., M.A. Wierzbicki, and D.J. Maitland, *Design and Characterization of a Resistively Heated Shape Memory Polymer Micro-Release Device1*. Journal of Medical Devices, 2014. **8**(2): p. 020911-020911.

25. Singhal, P., et al., *Controlling the Actuation Rate of Low-Density Shape-Memory Polymer Foams in Water.* Macromolecular Chemistry and Physics, 2013. **214**(11): p. 1204-1214.